Universiteit
Leiden
The Netherlands

Effects of heavy fields on inflationary cosmology

Ortiz, P.

Citation
Ortiz, P. (2014, September 30). *Effects of heavy fields on inflationary cosmology*. *Casimir PhD Series*. Retrieved from https://hdl.handle.net/1887/28941

Version:	Not Applicable (or Unknown)
License:	Leiden University Non-exclusive license
Downloaded from:	https://hdl.handle.net/1887/28941

Note: To cite this publication please use the final published version (if applicable).

Cover Page

Universiteit Leiden

The handle http://hdl.handle.net/1887/28941 holds various files of this Leiden University dissertation.

Author: Ortiz, Pablo
Title: Effects of heavy fields on inflationary cosmology
Issue Date: 2014-09-30

1

Cosmological inflation: its realisations and observables

In this first chapter I give an overview of cosmological inflation, which will gradually become more concrete and focused on the topics that are treated in depth in the remaining chapters. Thus, I provide the basic ingredients necessary to follow the articles [1–4] presented in the main body of this thesis. Throughout this manuscript, unless specified, I will work in units of $\hbar = c = 1$ and will set the Planck mass to $M_p = (8\pi G)^{-1/2} = 1$.

1.1 Introduction: an expanding universe

Cosmological inflation is a paradigm that was invented over thirty years ago [5–10]. It is defined as an era of accelerated expansion of the very early universe. The key observation that led to this idea was that the universe is highly homogeneous and isotropic on large scales. This was an assumption that physicists called "cosmological principle" and that was later confirmed by the observation of the Cosmic Microwave Background (CMB) radiation by Penzias and Wilson [11] in 1965. This radiation is, roughly speaking, a picture of the photon temperature distribution in two dimensions corresponding to the time when the photons decoupled from the hot plasma (380000 years after the 'Big Bang'), as I will explain in detail in section 1.3. The spectrum of this radiation is that of a perfect black body with temperature 2.73K, and deviations from this average temperature are only of one part in 10^5.

An important question that comes when observing such a homogeneous radiation was that, patches of the universe that in principle were never causally connected have the same temperature, how is this possible? If gravity was always

attractive, then the initial size of the universe would be larger than the causally connected patch at that time. Given the observations, the initial state of the universe should be such that all the causally disconnected regions have roughly the same temperature. Either the initial conditions were inexplicably given just like that, or there is a mechanism underneath that explains them. Of course physicists pursued the second alternative.

In addition to the high degree of homogeneity and isotropy, the universe is extremely flat, which is also very unnatural for a decelerating universe, since it is an unstable stage. Having seen this, it seems rather natural to ask which initial conditions led to such a 'perfect' universe. The main motivation for inflation was to propose a mechanism such that these characteristics were *predicted*, rather than accepted as very unlikely initial conditions, and it turns out that inflation has succeeded tremendously in this respect. In this thesis I will not focus on the detailed description of the initial condition problems, and refer to those interested in them to the excellent reviews and textbooks [12–16]. The key feature of inflation that solves these problems of initial conditions is the accelerated expansion. Furthermore, we will see that inflation yields the generation of primordial density perturbations, which explain the tiny inhomogeneities of the CMB temperature, and that later on generated the large scale structure observed nowadays.

The plan of this chapter is the following: I will briefly review the geometry of an expanding universe and the conditions for an accelerated expansion. The natural candidate to drive such an expansion is a scalar field, whose quantum fluctuations originate the primordial density perturbations that seeded the growth of structure, as I will explain at the beginning of section 1.2. The correlation functions of the primordial curvature perturbation contain valuable information that remains frozen for a long time and whose evolution can be tracked down until the time when the CMB is emitted, which allows us to study the footprints of the quantum fluctuations during inflation. At the end of section 1.2 I provide the standard well-known predictions for the two- and three-point correlation functions. But one of the most important successes of inflationary cosmology is the predictive power and the stunning agreement with CMB measurements. Especially in the last decade cosmologists have been very fortunate to count on the WMAP, Planck and BICEP experiments, which have given us the opportunity to test our theories. In section 1.3 I briefly explain the physics of the CMB, I will review the (very exciting) current experimental status, and I will explain how the CMB data help us constraining the incredible amount of inflationary models. We will see that there is still much room for a rich variety of inflationary setups, and in particular I have explored in this thesis the effect of additional degrees of freedom, which naturally arise in UV completable theories. Therefore, it is natural to ask ourselves whether it is possible or not to detect, and under which circumstances, those additional particles that play inflation

along with the inflaton. In section 1.4 I focus on inflationary scenarios embedded in supergravity and the tools that enable us to give a simpler, yet consistent, theoretical description. Finally, in section 1.5 I explain how the inflaton field feels the presence of additional heavy fields and how this affects the observable predictions.

1.1.1 The Friedmann - Lemaître - Robertson - Walker universe

The series of works [17–22] gave name to what we know today as the Friedmann-Lemaître-Robertson-Walker (FLRW) universe. It is basically described by a space-time that is homogeneous and isotropic for each time slice, with distance between two comoving observers proportional to the scale factor $a(t)$. The line element in the FLRW metric can be written in spherical coordinates as follows:

$$ds^2 = g_{\mu\nu}dx^\mu dx^\nu = -dt^2 + a^2(t)\left[\frac{dr^2}{1-kr^2} + r^2\left(d\theta^2 + \sin^2\theta\, d\phi^2\right)\right] , \quad (1.1.1)$$

where k gives the spatial curvature, as can be read from the spatial Ricci scalar $R^{(3)} = 2k/a^2$. The constant k can take values $+1, -1$ and 0, that describe space-times with positive curvature, negative curvature, and flat, respectively. Since all the observations are in excellent agreement with a flat universe, in this thesis I will only describe flat FLRW space-times with $k = 0$, which in cartesian coordinates can be simply written as:

$$ds^2 = -dt^2 + a^2(t)\left(dx^2 + dy^2 + dz^2\right) . \quad (1.1.2)$$

An important quantity derived from the scale factor is the Hubble parameter

$$H(t) \equiv \frac{\dot{a}}{a} , \quad (1.1.3)$$

which measures the expansion rate of the universe. Along this manuscript, for convenience I will often measure time using the conformal time $\tau \equiv \int dt/a(t)$,[1] in terms of which the FLRW metric is conformally flat, which means that it can be expressed as a conformal transformation of the Minkowski metric. Then, using the conformal time the metric reads:

$$ds^2 = a^2(\tau)\left(-d\tau^2 + dx^2 + dy^2 + dz^2\right) . \quad (1.1.4)$$

This settles the description of the space-time in which inflation occurs. The other essential ingredient we need to describe the cosmology is the matter, which is

[1] The conformal time is usually written as η instead of τ, but I will reserve the former to denote the second order slow-roll parameter that will appear repeatedly in the text.

specified through the energy-momentum tensor $T_{\mu\nu}$. The energy (or matter) content and the geometry of the space-time satisfy the Einstein equations:[2]

$$G_{\mu\nu} \equiv R_{\mu\nu} - \tfrac{1}{2} g_{\mu\nu} R - \Lambda g_{\mu\nu} = T_{\mu\nu} \ , \tag{1.1.5}$$

where $R_{\mu\nu}$ is the Ricci tensor, R is the Ricci curvature scalar, and Λ is the cosmological constant term. The Λ-term represents the vacuum energy and can always be written as a constant contribution to the energy momentum tensor, thus from now on I will set $\Lambda = 0$, and later on the cosmological constant will be often given by the value of the scalar potential at the vacuum.

On large scales the cosmic fluid is well approximated by a perfect fluid, characterised by its energy density ρ, pressure p, and velocity u^μ, and for which the energy-momentum is

$$T^{\mu\nu} = (p + \rho) u^\mu u^\nu + p\, g^{\mu\nu} \ . \tag{1.1.6}$$

The conservation of the energy-momentum tensor follows from the Bianchi identities applied to the Einstein tensor $G_{\mu\nu}$, which in terms of energy and pressure gives the continuity equation:

$$\dot{\rho} = -3H(p + \rho) \ , \tag{1.1.7}$$

which is nothing else than the conservation of energy for a perfect fluid in a homogeneous and isotropic universe. In addition to the previous equation, the Einstein equations (1.1.5) for a FLRW universe filled with a perfect fluid characterised by eq. (1.1.6) are well known as the Friedmann equations, which read:

$$H^2 = \left(\frac{\dot{a}}{a}\right)^2 = \frac{\rho}{3} \quad , \qquad \dot{H} + H^2 = \frac{\ddot{a}}{a} = -\frac{1}{6}(\rho + 3p) \ . \tag{1.1.8}$$

One can combine the previous equations to obtain a very useful expression:

$$\dot{H} = -\frac{1}{2}(p + \rho) \ . \tag{1.1.9}$$

It is clear then that once the equation of state of the fluid $p(\rho)$ is given, the evolution of the scale factor $a(t)$ and of the fluid are determined. The most interesting situations in cosmology are characterised by $p = w\rho$. For instance, for radiation one has $w_{\rm rad} = 1/3 \Rightarrow \rho_{\rm rad} \sim a^{-4}$, for matter $w_{\rm mat} = 0 \Rightarrow \rho_{\rm mat} \sim a^{-3}$, and for vacuum energy or a cosmological constant $w_\Lambda = -1 \Rightarrow \rho_\Lambda \sim$ const. Notice that the universe is (positively) accelerated when

$$w < -\tfrac{1}{3} \quad \Rightarrow \quad \ddot{a} > 0 \quad \text{(inflation)} \ . \tag{1.1.10}$$

An accelerated expansion solves the homogeneity puzzle, as illustrated in figure

[2] See appendix A for conventions.

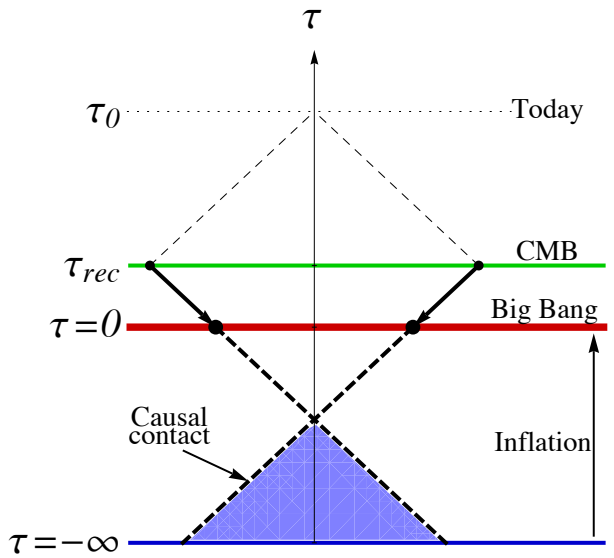

Figure 1.1 *– Diagram illustrating the solution to the horizon problem. If there exists a sufficiently long period of accelerated expansion before the Big Bang, two apparently disconnected regions were in reality connected before. This explains why the CMB radiation has an almost perfectly uniform temperature distribution.*

1.1, because it makes possible the creation of our universe from a causally connected domain, even if outside this domain the universe is initially very inhomogeneous. This is because the physical size of the perturbation grows faster than the curvature scale (H^{-1}). Due to the same reason, the flatness problem is also solved by a period of accelerated expansion. The evolution of the curvature dictates that positive acceleration drives the curvature to zero, and becomes an attractor of inflation.

By inspecting the Friedmann equations (1.1.8) one can see that $p < -\rho/3$ produces an accelerated expansion. One could first consider $H = \text{const}$ and therefore exponential expansion. However, perfect exponential expansion would never end, so we will need small deviations that will be parameterised by

$$\epsilon \equiv -\frac{\dot{H}}{H^2} \ , \tag{1.1.11}$$

such that the condition for an accelerated universe translates now into $\epsilon < 1$. Inflation must last sufficiently long to stretch a small domain to the size of the observable universe, and also to flatten the possible initial inhomogeneities to the level observed in the CMB. The duration or amount of inflation is usually measured as a function of the *number of e-folds*, N, which is roughly speaking

the amount of times that the universe expands by a factor e, and its definition is:

$$dN = H\,dt = \frac{da}{a}\ . \tag{1.1.12}$$

Typically the solution of the flatness and horizon problems demands an amount between 60 and 70 e-folds of inflation. This also implies that the value of ϵ at the beginning of inflation should be approximately one percent or less. In the next section we will see how we can achieve accelerated expansion long enough.

1.2 Inflating the universe with a scalar field

The natural candidate to drive inflation is a scalar field ϕ, which easily describes the energy density and pressure of a perfect fluid in terms of its kinetic energy and a scalar potential $V(\phi)$. In this case the field ϕ drives inflation and is therefore called the *inflaton*. If one takes the action for a scalar field in a FLRW metric and calculates the energy-momentum tensor, it is easy to see that the energy density and the pressure are given by:

$$\rho = \tfrac{1}{2}\dot{\phi}^2 + V(\phi) \quad , \qquad p = \tfrac{1}{2}\dot{\phi}^2 - V(\phi)\ . \tag{1.2.1}$$

Also, the equation of motion for a homogeneous scalar field in a FLRW background is

$$\ddot{\phi} + 3H\dot{\phi} + V_\phi = 0\ , \tag{1.2.2}$$

where the subindex in V_ϕ denotes derivative with respect to the scalar field.

Slow-roll conditions

Let us make a brief interlude to define the slow-parameters that must be small in order to achieve a sufficiently large amount of inflation. As can be seen from eq. (1.1.9), the universe undergoes quasi-exponential expansion if the equation of state of the fluid is $p \simeq -\rho$, which in view of (1.2.1) translates into

$$\tfrac{1}{2}\dot{\phi}^2 \ll V(\phi) \quad \text{(slow-roll)}\ . \tag{1.2.3}$$

Since the kinetic energy must be much smaller than the potential, the name slow-roll is obvious. Using the Friedmann equations (1.1.8) and substituting the energy density and pressure for our scalar field (1.2.1), one clearly sees that slow-roll requires $\epsilon \ll 1$ for a sufficiently large amount of time. The condition of small ϵ lasting long enough is usually expressed in terms of a second slow-roll parameter η, however in the literature there is no clear consensus on how to define this parameter[3]. Some of the alternatives that make sense are the following:

$$\eta_1 = -\frac{\dot{\epsilon}}{H\epsilon} \quad , \qquad \eta_2 = -\frac{\ddot{H}}{H\dot{H}} \quad , \qquad \eta_3 = -\frac{\ddot{\phi}}{H\dot{\phi}}\ . \tag{1.2.4}$$

[3]When dealing with multiple scalar fields, there are even more possible definitions, as I will explain in section 1.5.1.

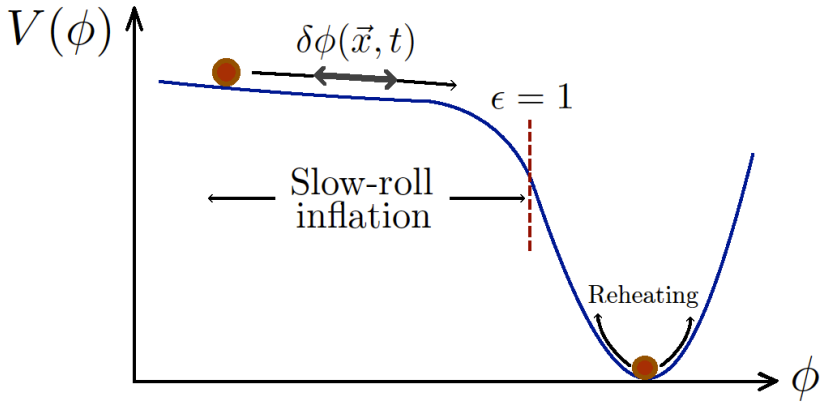

Figure 1.2 *– Typical scalar potential for slow-roll inflation. Accelerated expansion (inflation) ends when $\epsilon = 1$, and reheating starts when the inflaton oscillates around the minimum.*

The first two are related through the equality:

$$\eta_1 = \eta_2 - 2\epsilon \ . \tag{1.2.5}$$

There is still an alternative definition of the first slow-roll parameter ϵ in terms of the scalar potential. This definition is somewhat intuitive since it involves the slope of the potential, which must be very small compared to the height of the potential, and therefore one can define

$$\epsilon_V \equiv \frac{1}{2}\left(\frac{V_\phi}{V}\right)^2 = \epsilon\left(\frac{3-\eta_3}{3-\epsilon}\right)^2 \ . \tag{1.2.6}$$

Let me make an important point here. In the above expression, it is clear that the usual slow-roll limit $\epsilon, \eta_3 \ll 1$ implies $\epsilon_V \simeq \epsilon \ll 1$, but it is important to notice that the opposite is not true. In fact, one can have $\epsilon > 1$ and still get $\epsilon_V < 1$. In this thesis I will always be using the kinematical parameter ϵ instead of the potential parameter ϵ_V.

For completeness, I will define yet another potential slow-roll parameter which has to do with the curvature of the scalar potential. The same way that for slow-roll one needs a small slope, for it to last long enough one needs small curvature, and therefore it is convenient to define

$$\eta_V \equiv \frac{V_{\phi\phi}}{V} = \frac{3}{3-\epsilon}\left[\epsilon + \left(1 - \frac{\xi}{3}\right)\eta_3\right] \quad , \qquad \text{with} \quad \xi \equiv -\frac{\dddot{\phi}}{H\ddot{\phi}} \ , \tag{1.2.7}$$

which will actually be more relevant for the multiple-field case, where it is related to the eigenvalues of the mass matrix coming from the Hessian of the potential.

This discussion will be enough to go on, and I will go into more subtleties later in the multiple-field case. Let us establish the standard single-field slow-roll conditions as $\epsilon, \eta_3 \ll 1$.

In the following I will consider the quantum mechanical picture of inflation, which is an essential step to describe the origin of primordial inhomogeneities.

1.2.1 Quantisation and mode equations

The fluctuations of the inflaton field can be written as $\delta\phi(\mathbf{x}, t) = \phi(\mathbf{x}, t) - \phi_0(t)$, with $\phi_0(t)$ the homogeneous part satisfying the background equation of motion (1.2.2). The spatial dependence is just telling us that different regions of the universe will inflate by slightly different amount, which will produce fluctuations in the local densities and eventually originate the temperature fluctuations of the CMB. Let us write the action for the inflaton field:

$$S = \int d^4x\, a^3(t) \left[\frac{1}{2}R - \frac{1}{2}g^{\mu\nu}\partial_\mu\phi\partial_\nu\phi - V(\phi)\right] . \tag{1.2.8}$$

When perturbing the action above, we find 5 scalar modes, responsible for the gravitational instability and structure formation, 4 vector modes, which decay very quickly and therefore are not important, and 2 tensor modes, which are the gravitational waves, whose analysis are out of the scope of this thesis. If we focus on the scalar modes, invariance under the transformations $t \to t + c_0$, $x_i \to x_i + \partial_i c$ remove two scalar modes. The Einstein equations remove two more scalar modes, and we are finally left with only one scalar degree of freedom. There are many different gauge choices, but we will just content ourselves with studying the *comoving gauge* [23], in which $\delta\phi = 0$, and thus the perturbations are put in the metric:

$$\delta g_{ij} = a^2(1 - 2\zeta)\delta_{ij} + \text{grav. waves} , \tag{1.2.9}$$

where ζ is the so-called *curvature perturbation*, since the spatial curvature scalar is $R_{(3)} = 4\nabla^2\zeta/a^2$. The beauty of this gauge resides in the fact that it explicitly exposes the conservation of the curvature perturbation on large scales outside the Hubble horizon (superhorizon scales), that is:

$$\dot{\zeta}_{\mathbf{k}} = 0 \qquad \text{for} \quad k \ll aH . \tag{1.2.10}$$

A careful treatment of the perturbed Einstein equations is not relevant for this thesis, and the purpose of this subsection is just to show the quadratic action in terms of the canonical variables. Thus, I will assume that we have solved the perturbed Einstein equations, rewritten the quadratic action in conformal time, and changed variables to obtain canonical kinetic terms. This leads to the following quadratic action:

$$S_2 = \frac{1}{2}\int d\tau\, d^3\mathbf{x} \left[v'^2 - (\nabla v)^2 + \frac{z''}{z}v^2\right] , \tag{1.2.11}$$

where the prime denotes derivative with respect to conformal time, and $v = z\zeta = a\sqrt{2\epsilon}\,\zeta$. This action can be seen as that of a harmonic oscillator with a time-dependent mass. Expanding in creation and annihilation operators:

$$v(\tau,\mathbf{x}) = \int \frac{d^3\mathbf{k}}{(2\pi)^{3/2}} \left[a^-_{\mathbf{k}} v_k(\tau) \mathrm{e}^{i\mathbf{k}\cdot\mathbf{x}} + a^+_{\mathbf{k}} v^*_k(\tau)\mathrm{e}^{-i\mathbf{k}\cdot\mathbf{x}}\right] . \tag{1.2.12}$$

Now we can promote v, its canonical conjugated momentum π, and a^-, a^+ to operators, such that

$$[\hat{v}(\tau,\mathbf{x}),\hat{\pi}(\tau,\mathbf{y})] = i\delta(\mathbf{x}-\mathbf{y}) \quad , \qquad \left[\hat{a}^-_{\mathbf{k}},\hat{a}^+_{\mathbf{k}'}\right] = \delta(\mathbf{k}-\mathbf{k}') \tag{1.2.13}$$

are the canonical commutation relations. We will assume from now on that they are operators and drop the hats. Now that we have quantised the system, let us derive the equations of motion in Fourier space from the action (1.2.11):

$$v_k''(\tau) + \left(k^2 - \frac{z''}{z}\right) v_k(\tau) = 0 . \tag{1.2.14}$$

This is called the Mukhanov-Sasaki equation [24, 25]. For the simplest case of a quasi-de Sitter universe with $\epsilon \simeq \text{const} \ll 1$, we have $z''/z \simeq 2/\tau^2$, where we have used $\tau \simeq -(aH)^{-1}$. [4] Before displaying the solution, let us fix the initial conditions, and the standard choice is to impose that for $\tau \to -\infty$ (beginning of inflation) the mode function corresponds to a Minkowski state:

$$\lim_{\tau\to-\infty} v_k(\tau) = \frac{1}{\sqrt{2k}}\mathrm{e}^{-ik\tau} . \tag{1.2.15}$$

This is known as the Bunch-Davies vacuum [26], and although other choices are possible and are actually endowed with a rich phenomenology (for instance, see [27–30]), in this thesis I will always consider a Bunch-Davies vacuum state. Then, the solution to the mode equation is

$$v_k(\tau) = \frac{\mathrm{e}^{-ik\tau}}{\sqrt{2k}}\left(1 - \frac{i}{k\tau}\right) . \tag{1.2.16}$$

It can be easily checked that for subhorizon modes ($k \gg aH$) the curvature perturbation $\zeta = v/a\sqrt{2\epsilon}$ has oscillating solutions, while for superhorizon modes ($k \ll aH$) it is constant. The very important consequence of this is that the curvature perturbation remains frozen after crossing the Hubble horizon, which allows us to obtain information from the inflationary epoch by looking at the statistical properties of the CMB, as illustrated in figure 1.3. In what follows, I review the standard predictions of single-field slow-roll inflation for the two- and three-point functions of the curvature perturbation, also known as the primordial power spectrum and bispectrum.

[4] A much more general and detailed treatment will be given in chapter 3, where we consider non-canonical kinetic terms and deviations from the quasi-de Sitter stage. However, the zero order solutions displayed here are the pillar over which more general solutions are constructed.

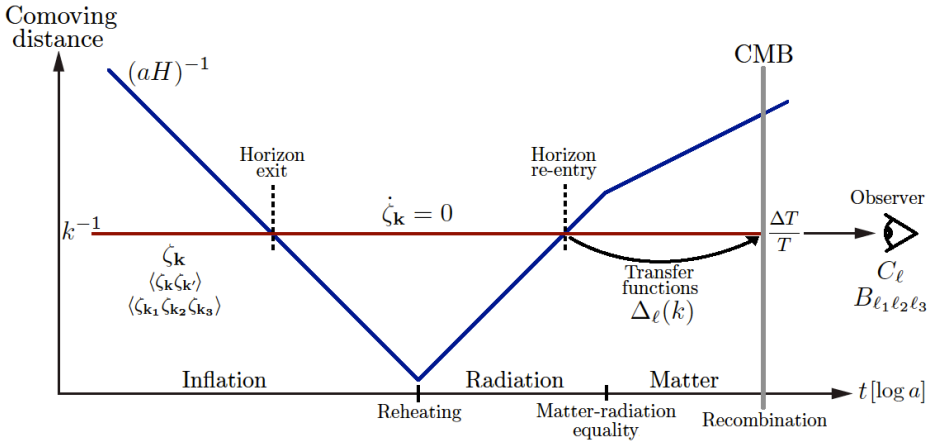

Figure 1.3 – *Scheme of the evolution of the comoving Hubble horizon (blue) in relation to perturbations of a given wavelength (red). During inflation the perturbations exit the horizon and remain frozen, and after reheating they re-enter the horizon, preserving the information of the inflationary epoch. Then they evolve together with the photon-baryon fluid, and the density perturbations leave their imprints on the photon temperature distribution, that is observed in the CMB when the photons are released. Figure adapted from [13].*

1.2.2 Standard predictions: correlation functions

Once we have the solution of our mode equations (1.2.14), it is possible to calculate the correlation functions of the adiabatic curvature perturbation $\zeta_{\mathbf{k}}$. Any distribution, and in particular that of the CMB temperature, is completely specified by its correlation functions. As it happens, the CMB temperature distribution is almost gaussian as far as we know [31, 32], and therefore the two-point function, i.e. the power spectrum, almost completely specifies the spectrum of perturbations. However, the three-point function (bispectrum) and higher order correlation functions play an important role in breaking degeneracies among different inflationary models, and therefore it is important to know as much as possible about them, even if they are small, because they represent departures from a perfect gaussian spectrum. The definitions of the primordial power spectrum and bispectrum are:

$$\langle\zeta_{\mathbf{k}}\zeta_{\mathbf{k}'}\rangle \equiv (2\pi)^3\delta(\mathbf{k}+\mathbf{k}')\,P_\zeta(k)\ , \tag{1.2.17}$$

$$\langle\zeta_{\mathbf{k_1}}\zeta_{\mathbf{k_2}}\zeta_{\mathbf{k_3}}\rangle \equiv (2\pi)^3\delta(\mathbf{k_1}+\mathbf{k_2}+\mathbf{k_3})\,B_\zeta(\mathbf{k_1},\mathbf{k_2},\mathbf{k_3})\ . \tag{1.2.18}$$

It is often convenient to define the dimensionless scalar power spectrum

$$\mathcal{P}_\mathcal{R}(k) \equiv \frac{k^3}{2\pi^2}P_\zeta(k)\ . \tag{1.2.19}$$

The power spectrum can be evaluated at horizon crossing, i.e. $k = aH$, since the curvature perturbation freezes then. Taking the solution to the mode equations (1.2.16) and performing the commutation operations in terms of creation and annihilation operators, one finally obtains [26]:

$$\mathcal{P}_{\mathcal{R}}(k) = \left.\frac{H^2}{8\pi^2\epsilon}\right|_{k=aH} , \tag{1.2.20}$$

which is scale-invariant except for the slight time dependence of H^2 and ϵ. To evaluate this scale dependence one can do the following computation [33]:

$$n_s - 1 \equiv \frac{d\ln\mathcal{P}_{\mathcal{R}}}{d\ln k} \simeq -2\epsilon + \eta_1 + \mathcal{O}(\epsilon^2) , \tag{1.2.21}$$

where I have neglected higher order slow-roll corrections. The scalar *spectral tilt* n_s measures the deviation of the scalar power spectrum from scale invariance. The deviation from scale invariance is a strong probe of inflation, since that is one of its most general predictions, and furthermore $n_s < 1$ also indicates that inflation comes to an end. It has been recently confirmed by the Planck collaboration [34] with more than 5σ c.l. that this is the case:

$$n_s = 0.9603 \pm 0.0073 \quad (1\sigma \text{ c.l.}) . \tag{1.2.22}$$

Later in section 1.3 I will go into the details of the experimental status regarding the power spectrum and bispectrum measurements. Since n_s is roughly speaking an 'average' of the tilt of the power spectrum, oscillations on top of the flat shape are allowed, and as we will see in chapters 2 and 3, these features may come together with some other interesting predictions for the bispectrum. The possibility of having non-trivial shapes fitting the data better than the standard result reviewed above is worth exploring in detail, since it may hint at additional degrees of freedom apart from the inflaton.

As for the primordial bispectrum, I will review the main results and leave further details for chapter 3, where I compute in full detail the complete bispectrum for a feature model. The first estimations of the bispectrum in slow-roll single-field models were given in [35–38], while the complete calculation was made in [39]. In these works it was stated that the bispectrum is of order of the slow-roll parameters and therefore very suppressed.

In order to calculate the bispectrum one has to expand the action in fluctuations of the inflaton field $\delta\phi$ around the homogeneous solution ϕ_0 to cubic order, where the non-linearities (interactions) arise. The expectation value we want to calculate can be computed using the *in-in formalism* [40, 41] and is given by:

$$\langle\zeta^3\rangle = \langle U_{\rm int}^{-1}\zeta^3 U_{\rm int}(t,t_0)\rangle \quad , \qquad U_{\rm int} = T\exp\left[-i\int_{t_0}^{t} dt'\, H_{\rm int}(t')\right] , \tag{1.2.23}$$

where $H_{\rm int}$ is the interaction Hamiltonian, which for the cubic terms equals $-L_{\rm int}$. Taking the first order approximation for the exponential above, the expectation value is then

$$\langle\zeta^3\rangle = -i\int_{t_0}^{t} dt' \left\langle\left[\zeta^3(t'), H_{\rm int}(t')\right]\right\rangle . \tag{1.2.24}$$

After a lengthy calculation[5], one obtains the following result [39]:

$$B(k_1,k_2,k_3) = \frac{(2\pi)^4 {\mathcal{P}_{\mathcal{R}}}^2 \epsilon}{8k_1^3k_2^3k_3^3}\mathcal{A} , \tag{1.2.25}$$

where

$$\mathcal{A} = (1-\frac{2\eta_3}{\epsilon})\sum_i k_i^3 + \sum_{i\neq j} k_i k_j^2 + \frac{8}{K}\sum_{i>j} k_i^2 k_j^2 , \tag{1.2.26}$$

and $K \equiv k_1+k_2+k_3$. This result implies that the bispectrum in the standard single-field slow-roll paradigm is suppressed by the slow-roll parameters. There are different scenarios that depart from these simplest models, for instance non-Bunch-Davies initial vacuum state, non-canonical kinetic terms, sharp steps in the scalar potential, or multiple fields during inflation can in principle enhance the non-gaussianity. As I will show in chapters 2 and 3, the influence of heavy fields during inflation may give rise to scale-dependent features in the power spectrum and bispectrum that are in reasonable agreement with the CMB data. In the next section I explain how from the CMB temperature anisotropies we can extract information about the quantum fluctuations of the inflaton field, and I will give an overview of the current experimental status.

1.3 The Cosmic Microwave Background Radiation

The CMB radiation is a tremendously exciting subject for early universe cosmologists, since it contains the footprints of inflation. In this section I give a qualitative explanation on how and why this is the case, and a more precise discussion on this issue can be found for instance in [42]. Although the details of the physical processes involved and the precise results are not essential for the rest of this thesis, I believe that is important to posses a qualitative understanding of the CMB physics in order to comprehend the relevance of the results presented in the following chapters. Throughout this section I will often refer to a sketch of the different eras involved in the transition from inflaton fluctuations to CMB temperature anisotropies, shown in figure 1.3. I will describe the events and physical phenomena that explain the shape of the temperature spectrum, and

[5] In chapter 3 I explain in detail the procedure that one must follow to calculate the bispectrum using the in-in formalism. Although the calculation is performed for a particular feature model, the same methodology applies to any case.

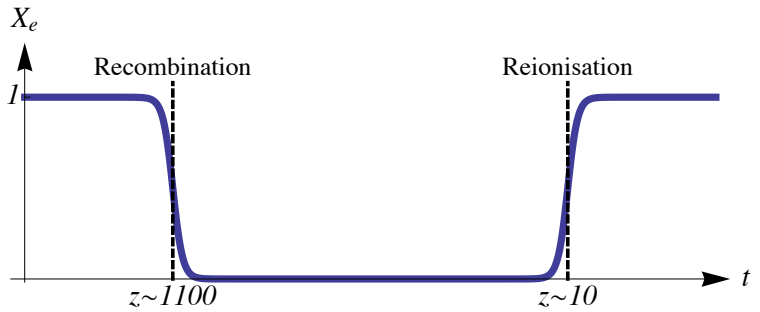

Figure 1.4 *– Fraction of ionised hydrogen atoms as a function of time. At recombination, hydrogen is neutralised and the photons can travel freely, then the CMB is emitted. When stars are formed, the UV photons emitted from them reionise the universe, but it has already diluted enough so that only about 10% of the CMB photons scatter, as parameterised by the optical depth.*

in the last part I will review the experimental status of power spectrum and bispectrum measurements.

Right after the Big Bang, the universe is at such a high temperature that hydrogen is ionised, which in particular means that electrons are freely floating around. That is the reason why we cannot see the photons of that time, because they were scattering off those electrons and their mean free path was of a few centimetres. Eventually, after approximately 380000 years, the universe drops its temperature to about 0.3 eV, which is sufficiently low for the hydrogen atoms to bind, and therefore *recombination* occurs. The figure 1.4 illustrates this process. Then the mean free path of the photons rapidly increases and quickly becomes larger than the Hubble horizon. At this point the photons can travel freely towards us, this moment is known as *decoupling*. These are the CMB photons.

The CMB radiation as measured by the Planck collaboration [32] can be seen in figure 1.5. As mentioned in the beginning of this chapter, the remarkable property of this radiation is that the temperature is basically uniform, fluctuations being only of order $\Delta T/T \sim 10^{-5}$. This outstanding homogeneity can be explained by having a period of inflation before the Big Bang, as shown in figure 1.1: since recombination happens very close in time to the Big Bang, regions separated by more than two degrees in the sky do not have time to be in causal contact. Roughly speaking, what inflation does is to extend this period further to the past, so that these regions were in causal contact.

Now, if we look back at figure 1.3, in order to understand how the inflaton fluctuations translate into the CMB temperature anisotropies, one has to follow the evolution of dark matter and the photon-baryon fluid in the presence

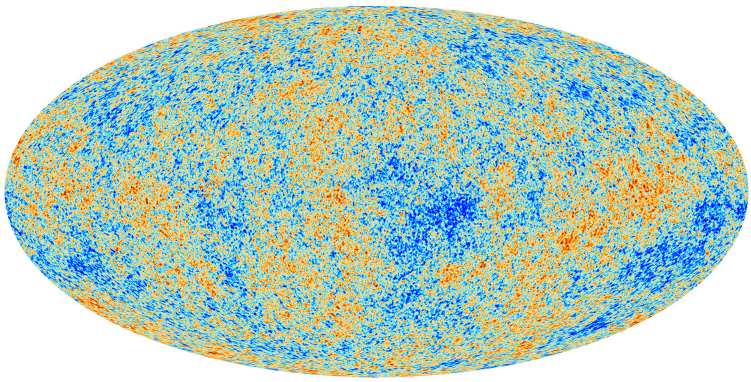

Figure 1.5 *– CMB temperature anisotropies as measured by the Planck collaboration, released on 21 March 2013 [32]. The temperature fluctuations are of one part in 100000, and the statistical properties of the distribution contain unique information about quantum fluctuations during inflation.*

of gravity throughout the radiation and matter eras. Basically, the inflaton fluctuations can be written in terms of metric perturbations, as we saw in eq. (1.2.9). Therefore, before recombination, the density and velocity of the baryon-radiation plasma will oscillate according to an equation for a harmonic oscillator in the presence of a gravitational potential. The beautiful physics involved is governed by the Boltzmann equation, the continuity equation and the Euler equation for our cosmic fluid. The CMB temperature distribution is then given as a function of the gravitational potential, the photon density fluctuations, and the velocity of the baryon-radiation plasma at recombination, which are at the same time determined by the inflationary perturbations, the Hubble constant, and the densities of baryons, cold dark matter, and dark energy.

All these effects can be effectively implemented by the *transfer functions*, which incorporate the evolution of the density perturbations between the times of horizon crossing and recombination. These are normally calculated with computer programs, as we did in the works presented in chapters 2 and 3, however in this section the aim is to provide an insight on the physics that determines the evolution from primordial to CMB anisotropies.

When observing the temperature fluctuations, we expand in spherical harmonics, which is the most natural way to decompose a two dimensional distribution:

$$\frac{\delta T}{T}(\Omega) = \sum_{\ell,m} a_{\ell m} Y_{\ell m}(\Omega) \quad \Rightarrow \quad a_{\ell m} = \int d\Omega \, Y^*_{\ell m}(\Omega) \frac{\delta T}{T}(\Omega) \ , \tag{1.3.1}$$

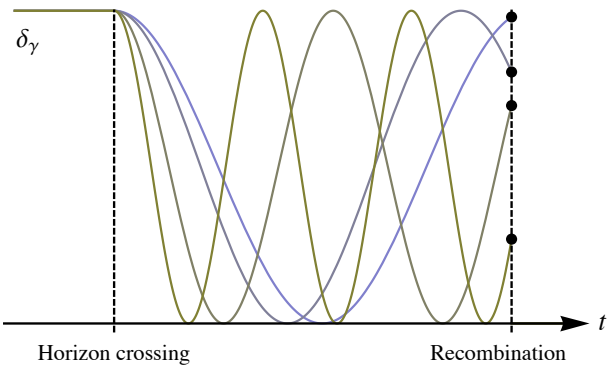

Figure 1.6 *– Photon density fluctuations since the metric perturbations re-enter the horizon until recombination. All the wavelengths start with the same phase because the photon density fluctuations are proportional to the curvature perturbation, which is frozen on superhorizon scales. The peak structure of the CMB power spectrum is partly due to this, otherwise the fluctuations of different wavelengths would be randomly distributed and they would average to zero, giving no peaks at all.*

and the CMB power spectrum is therefore determined by

$$C_\ell = \frac{1}{2\ell+1}\sum_m \langle a^*_{\ell m} a_{\ell m}\rangle \ . \tag{1.3.2}$$

The CMB power spectrum as measured by Planck [34] is showed in figure 1.7. One of the aims of this section is to explain the relationship between the primordial power spectrum (1.2.20) and the CMB power spectrum (1.3.2). In the following, I give a rough description of the physics that determines the several peculiarities of the CMB power spectrum (see figure 1.7), and a more detailed treatment of the subject can be found for instance in [15].

First of all, the peak structure is due to the fact that photon energy density fluctuations are proportional to the curvature perturbation. As argued above, the curvature perturbation remains frozen on superhorizon scales, and therefore when it re-enters the Hubble horizon, all photon wavelengths oscillate with the same phase. This behaviour is exemplified in figure 1.6. The same argument applies to the gravitational potential and photon velocities. If this were not the case, i.e. if the perturbations originated inside the horizon, the phases would be randomly distributed and they would average to zero, destroying then the peak pattern observed in the CMB temperature spectrum (see figure 1.7).

Second, there is an important transition happening in the first peak, that is the matter-radiation equality. As one can observe in figure 1.3, the first modes

exiting the Hubble horizon (low-k), will re-enter during the matter-dominated era. These modes contain more information about the inflationary era, since they do not have much time to evolve until recombination occurs, or no time at all. Unfortunately, the uncertainty for low ℓ measurements, known as *cosmic variance*, is large in this region. This uncertainty is due to the fact that we only have $2\ell + 1$ measurements for each ℓ, and therefore it is inevitable to have an error of $\Delta C_\ell / C_\ell \sim (2\ell + 1)^{-1/2}$. The maximum of the first peak corresponds to the matter-radiation equality, and subsequent modes of higher ℓ re-enter the horizon in the radiation-dominated era. Thus, these modes contain more information about the evolution of the cosmic fluid, and can be used to calibrate the *cosmological parameters* that characterise our cosmological model.

Another pattern we see in the peaks is that odd peaks are enhanced with respect to even peaks (before the exponential suppression, explained below), and moreover the valleys do not go down to zero. This is because the oscillating part of the CMB power spectrum contains two cosine functions[6], one having a period two times larger than the other, and therefore the odd peaks interfere constructively, while even peaks interfere destructively. However, since there is a relative phase shift between them, the interference is not perfect. In addition, the almost constant positive contribution represents the hydrostatic equilibrium inside the gravitational potential and enhances the whole spectrum.

Last, the peak structure is damped by two different phenomena: Silk damping and the finite thickness effect. The former is due to the fact that the photons can transfer energy from one region to another over distances determined by

[6] In order to see this, note that the temperature fluctuations observed at the present conformal time τ_0 coming from the direction $\mathbf{l}$ are given by [15]:

$$\frac{\delta T}{T}(\tau_0, \mathbf{x}_0, \mathbf{l}) = \int \frac{d^3k}{(2\pi)^{3/2}} \left[\left(\Phi + \frac{\delta}{4} \right)_{\mathbf{k}} - \frac{3\delta'_{\mathbf{k}}}{4k^2} \frac{\partial}{\partial \tau_0} \right]_{\tau_r} \mathrm{e}^{i\mathbf{k}[\mathbf{x}_0 + \mathbf{l}(\tau_r - \tau_0)]} \ ,$$

where τ_r is the conformal time at recombination, Φ the gravitational potential, and δ the radiation energy density fluctuation. When we calculate the average over all angular directions

$$C(\theta) = \left\langle \frac{\delta T}{T}(\mathbf{l}_1) \frac{\delta T}{T}(\mathbf{l}_2) \right\rangle = \frac{1}{4\pi} \sum_{\ell=2}^{\infty} (2\ell + 1) C_\ell P_\ell(\cos\theta)$$

and expand the sine function arising from the product of exponentials:

$$\frac{\sin\left[k|\mathbf{l}_1\tau_1 - \mathbf{l}_2\tau_2|\right]}{k|\mathbf{l}_1\tau_1 - \mathbf{l}_2\tau_2|} = \sum_{\ell=0}^{\infty} (2\ell + 1) j_\ell(k\tau_1) j_\ell(k\tau_2) P_\ell(\cos\theta) \ ,$$

we arrive at the following expression for the multipole moments:

$$C_\ell = \frac{2}{\pi} \int k^2 dk \left| \left[\Phi_k(\tau_r) + \frac{\delta_k(\tau_r)}{4} \right] j_\ell(k\tau_0) - \frac{3\delta'_k(\tau_r)}{4k} \frac{dj_\ell(k\tau_0)}{d(k\tau_0)} \right|^2 \ ,$$

which, when evaluated on small angular scales gives several non-oscillatory and oscillatory terms which result into the peak structure described in the text.

their mean free path. In other words, photons travel from hot to cold regions, mixing and scattering, with the final result of homogenising the temperature distribution and therefore this effect is seen as an exponential suppression[7]. As for the finite thickness effect, it refers to the finite duration of recombination. It is clear that due to this, there is an uncertainty as to the precise moment when a given photon last scatters. This affects inhomogeneities with scales smaller than the duration of recombination, which will be therefore strongly suppressed[8].

In summary, all these effects can be estimated analytically [42] in terms of cosmological parameters: the amplitude and spectral tilt of the primordial power spectrum, the Hubble constant today, the optical depth, the baryon and cold dark matter densities, the dark energy (or vacuum) density, and the curvature of the universe, which is rather assumed to be zero, in agreement with all experiments. In principle, the plateau for $\ell \ll 200$ and the first three acoustic peaks can determine most of the cosmological parameters. But including the damping scales introduces further dependence on the cosmological parameters and a precise determination of these requires the inclusion of higher peaks in the analysis. Moreover, there are several subdominant effects which I have not mentioned here, but that become relevant for very precise measurements of the CMB temperature spectrum and other observables. As mentioned before, the transfer functions that implement these effects are normally computed with Boltzmann solvers. Pioneering work on this subject was made in [43] and the two main codes used nowadays are CAMB [44] and CLASS [45, 46]. With all this rich phenomenology and tools at hand, one computes the CMB temperature fluctuations $\delta T/T$ given the initial conditions from inflation and the cosmological parameters. Then one compares the calculated CMB temperature spectrum in a given cosmological model to the observed one, and determines the cosmological parameters that reproduce the data best. In addition, one can test particular models of inflation where additional parameters are introduced, and find a fit for those parameters that reproduces well the data. In chapter 2 we present a well motivated model for which we performed this search.

Although there are another CMB observables, such as cross-correlated spectra and polarisation, I will focus on the power spectrum and bispectrum, which are the observables studied in this thesis. Regarding the bispectrum, the same physics determines its properties, as for the temperature spectrum. It is clear that the densities of baryons and cold dark matter, the optical depth, along with the expansion of the universe and the initial conditions coming from the inflationary era, are the ingredients that determine the evolution of the energy density of

[7] This suppression appears as a friction damping term in the equations of motion of the photon energy density fluctuations, that becomes important for scales of the order of the photon diffusion scale.

[8] The exponential suppression is the result of the infinite product of probabilities that a photon suffers Thomson scattering during the finite interval in which recombination occurs.

the photons and therefore the correlation functions of the CMB temperature distribution. In the next section I review the current status of power spectrum and bispectrum measurements, which will be relevant for chapters 2 and 3.

1.3.1 CMB power spectrum and bispectrum: experimental status

Let us now have a quick overview on the current status regarding the CMB power spectrum and bispectrum. First of all, the standard cosmological model ΛCDM is normally parameterised in terms of six cosmological parameters. On the one hand, the amplitude A_s and spectral index n_s of the primordial power spectrum. On the other hand, the primordial perturbations evolve in a flat FLRW universe parameterised by the densities of baryonic and cold dark matter, $\Omega_{\rm b}$ and $\Omega_{\rm cdm}$, and the current expansion rate H_0. The damping due to reionisation is parametrized by the optical depth $\tau_{\rm reio}$. For the analyses that we review here, the curvature is assumed to be zero, and the density of dark energy is then the critical density minus baryonic and cold dark matter densities. The latest data release by Planck [47] confirms once more that our universe is dominated by dark energy (68%), it has a substantial amount of cold dark matter (27%), and there is a small fraction of baryonic matter (5%). The precise results of these and the other cosmological parameters are given in [47].

So far, the data is in remarkable agreement with the baseline ΛCDM model, however the existence of certain anomalies in the power spectrum and bispectrum make us think that the baseline model might well be an effective description of a more complicated theory. More importantly, as I will show in chapters 2 and 3, an underlying theory able to predict not only features in the power spectrum and bispectrum, but also a direct correlation between them, would stand as a good candidate to describe the anomalies found in the data. Despite the existence of several data sets, I will focus on the latest results released by the Planck collaboration on the power spectrum [34] and the bispectrum [48], since they are the most precise at the time of writing this thesis.

The CMB power spectrum is shown in figure 1.7, which manifests the remarkable agreement between the data and the simple 6-parameter ΛCDM Planck baseline model [34]. Despite this, it also shows that there are many hints of anomalies between $50 < \ell < 1500$. The dip around $\ell = 1800$ has been questioned, since it seems to be only an effect coming from the 217×217 GHz map [49]. The uncertainties for $\ell < 50$ are not very significant due to the cosmic variance, as explained above. In chapter 2 we will see that models that produce localised oscillations can fit the data reasonably well [1], giving a prediction for the bispectrum that also seems to be in accordance with data.

Extracting primordial information from the CMB bispectrum is rather

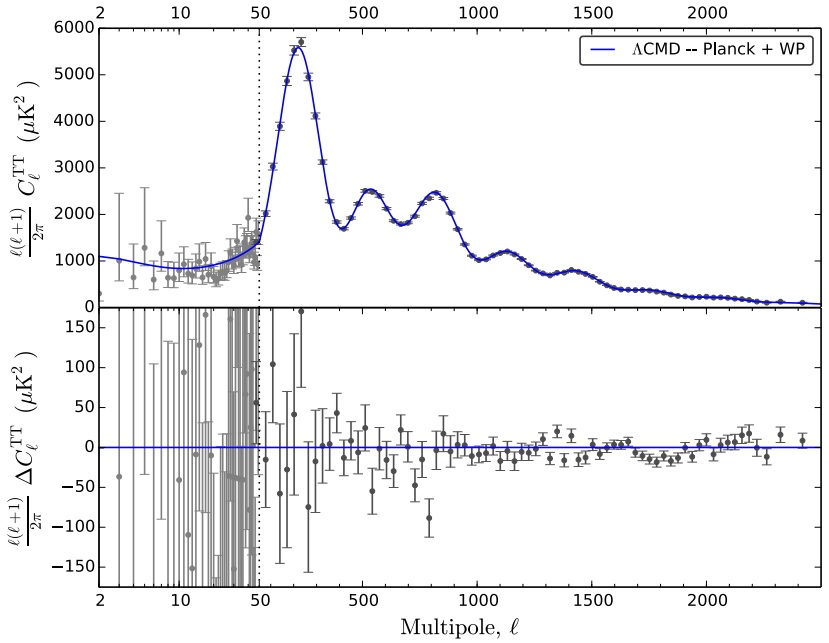

Figure 1.7 *– Planck data for the CMB power spectrum. The solid line represents the theoretical prediction of the Planck + WMAP polarisation baseline ΛCDM cosmological model. Note the series of hints of anomalies $> 1\sigma$ in the bottom plot, which measures the differences between the data points and the model.*

complicated, since there are three directions in ℓ-space. Thus, deconvolving the signal is computationally very challenging and the dependence on the parameters of the theory is much more intricate than for the power spectrum. Despite this, it is still possible to obtain some information on primordial non-gaussianity using the methods developed in [50–52]. The Planck collaboration performed several analyses on the bispectrum signal [48] that I shall briefly describe below.

It is worth noticing that a detection of non-gaussianity would be a smoking gun for models departing from the standard single-field slow-roll regime, since we saw in eq. (1.2.25) that for these models the bispectrum is strongly suppressed. One of the analysis of the Planck collaboration involves the search for primordial *scale-independent* non-gaussianity, parameterised by $f_{\rm NL}$. They looked for particular shapes of the triangle formed by the vectors $\{\mathbf{k_1}, \mathbf{k_2}, \mathbf{k_3}\}$, specifically for local, equilateral and orthogonal shapes, which form an almost orthogonal basis [53, 54], that is, they cover all the configuration space. They found that this type of

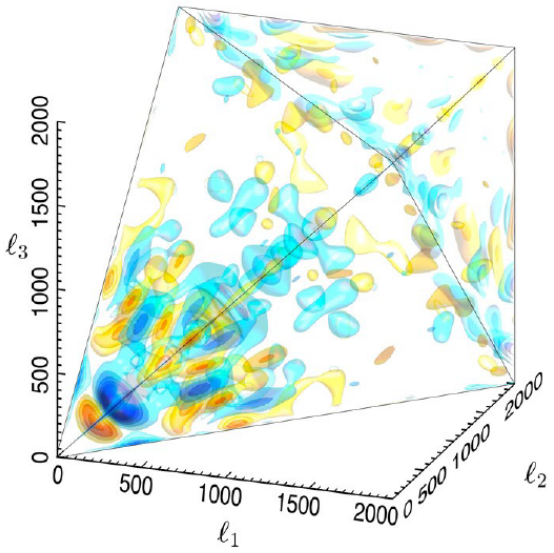

Figure 1.8 *– Reconstruction of CMB bispectrum from the Planck collaboration [48]. The red colour means positive values and blue colour negative values. This data reveals oscillations that are damped for* $\ell > 1500$.

non-gaussianity is small and consistent with zero:

$$f_{\rm NL}^{\rm loc} = 2.7 \pm 5.8 \quad , \quad f_{\rm NL}^{\rm eq} = -42 \pm 75 \quad , \quad f_{\rm NL}^{\rm orth} = -25 \pm 39 \qquad (1\sigma \text{ c.l.}) \, . \tag{1.3.3}$$

In addition, the Planck collaboration performed a search for *scale-dependent* bispectrum features [48], since the reconstruction of the CMB bispectrum data seems to indicate an oscillating signal, as shown in figure 1.8. Their search reveals anomalies of around 3σ with respect to a completely vanishing bispectrum. Although the search for scale-dependent features by Planck is analysed in detail in chapter 2, here I comment the main characteristics of their search. Essentially, they proposed primordial bispectrum templates with oscillations and computed the CMB bispectrum signal. Then they compare with the data and give the significance of their fits. Since this data is not public, the best attempt one can make to validate a bispectrum is to compare with their primordial templates. The Planck collaboration tested three types of primordial templates in the limit $k_1 = k_2 = k_3 = k$: linear oscillations in $\log k$, linear oscillations in k and linear localised oscillations with a gaussian envelope. As I will explain in detail in chapter 2, we proposed a feature model that predicts linear localised oscillations as well. As we will see, the underlying physical mechanism is consistent and well motivated, which justifies the introduction of additional parameters in the cosmological model. Interestingly enough, our functional form has a remarkable resemblance with theirs, and therefore we

were able to roughly test our templates using their analyses. The prospects are promising, since we found a reasonable agreement in our qualitative comparison [1].

Last, it is worth mentioning the recent striking results released by the BICEP2 collaboration [55], which claimed a detection of B-mode polarisation on degree scales that can be attributed to primordial gravitational waves. After this, the cosmology community has been (and still is) analysing all the possible consequences of this detection, but in my opinion these are not yet conclusive and the situation needs to settle down, therefore I prefer to keep a conservative approach. Among the most common arguments, one finds that if the BICEP2 results are confirmed, the inflaton field should have traversed transplanckian distances in order to produce a detectable tensor-to-scalar ratio [56], or in other words, primordial gravitational waves. However, the BICEP2 results have been questioned by several groups, see for instance [57, 58] for an analysis of the foregrounds. Therefore, in the absence of a robust confirmation, along this manuscript I take a cautious approach and consider these results as a possibility worth exploring and taking into account, but nevertheless the works presented in the following chapters do not aim to address the production of primordial gravitational waves.

Summarising, the present data confirms the most robust predictions of the standard inflationary paradigm with a single field and slow-roll regime. However, there is still room for more generic models as long as they predict observable features within the experimental bounds. If the hints of anomalies were confirmed by future data sets, it is important to provide a well-motivated underlying theory able to predict these features. Among these models, it is reasonable to propose inflationary setups which are embedded in UV completable theories, such as string theory of supergravity, since the energies at which inflation happens might be close to the Planck scale. In addition, the presence of additional fields (possibly representing the matter content) arises inevitably in these theories, fortunately or unfortunately. An alternative approach is to consider that new physics does not necessarily appear at high energies, and thus Higgs inflation models have been recycled from an old idea [59–62] by [63] and further studied, for instance, in [64–67]. Although this is a very well motivated scenario worth to explore, in this thesis we will discuss the possibility of having new physics.

In the next section I will review the characteristics of these UV embeddings and in particular the supergravity framework for inflation. Integrating out additional fields is subject to many subtleties that I will describe in the last section of this chapter, together with the possible observable features due to the presence of additional degrees of freedom.

1.4 UV completions of inflation

In this section we turn to more theoretical topics regarding the embedding of inflation in UV completable theories. It is natural to assume that given the energy scale at which inflation happens, a theoretical description that incorporates an UV completion is desirable. A great amount of work has been done in this direction, see for example the excellent reviews of inflation in string theory [68–71] (more recently [72]) and in supergravity [73–75].

From a theorist's perspective, embedding inflation in these theories might seem the natural thing to do. On the other hand, the great achievement of inflation lies on its predictive power, and therefore it is important to keep it as simple as possible, in line with Ockam's razor. Typically these theories introduce a large number of degrees of freedom and consequently a large number of parameters, losing their predictive power. In this situation one in principle has to face an inflationary setup with a large number of fields all coupled to each other, and still try to reduce the system to a simpler version which in the best case scenario can be studied analytically.

Let me stress that consistently integrating out or decoupling additional degrees of freedom is a far from trivial task. It is certainly not enough to argue that very heavy fields can be integrated out *à la Fermi* without consequences, because in a dynamical background there are plenty of effects which can excite these heavy degrees of freedom, invalidating the naive effective theory. In section 1.5 I will describe in detail the conditions for integrating out heavy fields consistently.

A complete review of the impressive amount of realisations of inflation in high-energy theories is out of range here, and therefore I will focus on the generic features of $\mathcal{N} = 1$ supergravity embeddings. In what follows I explain the peculiarities of the scalar potential in supergravity and what problems arise from the gravitational coupling. Details on the differential geometry concerning Kähler manifolds can be found in appendix A. A more self-contained and technical treatment of complex manifolds can be found for instance in [76]. I will focus on the phenomenological aspects of inflation in supergravity, for the formal aspects I refer to the reader to a pedagogical text on supergravity theories such as [77].

1.4.1 Inflation in $\mathcal{N} = 1$ supergravity

The bosonic part of the action for a set of N complex scalar fields Φ^a, $a = 1, \ldots, N$, is constructed with the Ricci scalar R, the kinetic terms of the scalar fields T and the scalar potential V:

$$S = \int d^4x\sqrt{-g}\left(\frac{1}{2}R + T - V\right) , \tag{1.4.1}$$

where g is the determinant of the space-time metric. In the absence of gauge fields, the couplings can be expressed entirely in terms of two functions of the scalars: the *Kähler potential* $K(\Phi, \bar{\Phi})$ and the holomorphic *superpotential* $W(\Phi)$. The fields Φ^a and their complex conjugates $\bar{\Phi}^{\bar{a}} = (\Phi^a)^*$ span a (complex) Kähler manifold whose metric is given by:

$$K_{a\bar{b}} = \frac{\partial^2 K}{\partial \Phi^a \partial \bar{\Phi}^{\bar{b}}} \ . \tag{1.4.2}$$

Unless specified, the partial derivatives with respect to Φ^a and $\bar{\Phi}^{\bar{a}}$ are denoted by subindices a and $\bar{a}$, and the metric $K_{a\bar{b}}$ and its inverse $K^{a\bar{b}}$ are used to raise and lower indices. The action (1.4.1) above can be expressed in terms of a single real scalar function combination of the Kähler potential and superpotential, the well known *Kähler function*, defined as:

$$G(\Phi, \bar{\Phi}) = K(\Phi, \bar{\Phi}) + \log |W(\Phi)|^2 \ , \tag{1.4.3}$$

which is well defined as long as $W \neq 0$. Throughout this manuscript, I will mostly use G instead of K and W, since the case $W = 0$ is not studied here. However, it is important to emphasise that the physical quantities, such as the scalar potential and its derivatives, are well defined for any value of the superpotential, and in some cases it will be interesting to take the limit $W \to 0$. In appendix A I provide a set of relations between quantities expressed in terms of G and in terms of K and W. The Kähler function is invariant under *Kähler transformations*:

$$K(\Phi, \bar{\Phi}) \to K(\Phi, \bar{\Phi}) + h(\Phi) + \bar{h}(\bar{\Phi}) \qquad \text{and} \qquad W(\Phi) \to W(\Phi) \mathrm{e}^{-h(\Phi)}, \tag{1.4.4}$$

with $h(\Phi)$ an arbitrary holomorphic function. In terms of the Kähler function, the kinetic terms and the scalar potential are given by:

$$T = G_{a\bar{b}}\, \partial_\mu \Phi^a \partial^\mu \Phi^{\bar{b}}, \qquad V = \mathrm{e}^G \left(G^a G_a - 3 \right) \ . \tag{1.4.5}$$

Supersymmetry is spontaneously broken when the expectation value of the supersymmetry transformations is non-zero, which for a bosonic configuration can only happen for the transformation of the chiral fermions χ^a:

$$\delta_\epsilon \chi^a = -\frac{1}{2}\, \mathrm{e}^{G/2} G^{a\bar{b}} G_{\bar{b}}\, \epsilon \ , \tag{1.4.6}$$

where ϵ is the parameter of supersymmetry transformations. Since the metric and the exponential are positive definite, the gradient of the Kähler function G_a defines a direction in field space known as the *sGoldstino* direction, which signals supersymmetry breaking. The sGoldstino corresponds to the supersymmetric partner of the would-be Goldstone fermion associated to broken supersymmetry.

In view of the above, when looking at the scalar potential in (1.4.5), one notices that in order to have inflation in supergravity we ought to break

supersymmetry, otherwise the scalar potential is negative and inflation cannot be realised. Therefore, there is always a sGoldstino direction in the field space. This will become relevant in chapter 4, where we identify the inflaton with the sGoldstino and study the possible regimes of inflation. Also, in both chapters 4 and 5 we use the projection of the mass matrix along the sGoldstino direction in order to get constraints on the stability of the fields.

Another characteristic feature of inflation in supergravity is the η-problem, which has to do with the second order slow-roll parameter given by the curvature of the potential, as in (1.2.7). Notice that the Kähler potential that gives canonical kinetic terms is of the following form[9]:

$$K = \Phi\bar{\Phi} \ . \tag{1.4.7}$$

The η-problem appears because of the exponential factor in the scalar potential. Due to this, the slow-roll parameter η_V reads:

$$\eta_V = 1 + \cdots \ , \tag{1.4.8}$$

hence the inflaton acquires an approximate mass of $\mathcal{O}(H)$ and slow-roll inflation does not last long enough. As will be described in more detail in chapter 4, there are possible ways out for this problem:

- For small field regimes one can always fine-tune the superpotential in such a way that the additional terms in $(\cdots)$ above conspire together to cancel the order unity contribution. This is not possible for large field regimes, since fine-tuning is not effective for a long trajectory.

- For large field regimes, one can invoke a symmetry, which is an elegant solution to provide flatness over a large trajectory. For instance, the Kähler potential in (1.4.7) has a flat direction for the phase, and therefore identifying the inflaton with the phase θ in $\Phi = |\Phi|e^{i\theta}$ would solve the η-problem. Several examples of different symmetries have been studied in [78–81]. The superpotential then introduces a soft breaking of the symmetry that produces the slope of the scalar potential.

Once the η-problem has been circumvented, we run into a more serious problem that in the literature is often assumed to be solved: the stabilisation of multiple fields. It is indeed a good first step to consider only one sector containing the inflaton, but what about considering the other sectors? Two potentially dangerous situations arise when considering additional fields: instabilities and isocurvature modes, both ruining the predictions of single-field inflation.

[9] Alternative forms related by a Kähler transformation are also possible, for instance one might have canonical kinetic terms for $K = \frac{1}{2}(\Phi + \bar{\Phi})^2$ or $K = -\frac{1}{2}(\Phi - \bar{\Phi})^2$.

1.4.2 Decoupling in supergravity

After taking care of the inflaton sector and making sure that the slow-roll conditions can be satisfied, one has to deal with the additional sectors. In order to solve the stability problems it is necessary to guarantee that the rest of fields remain *at least* heavy and stabilised during inflation. Even in that situation, it is still possible to see their influence in the CMB if they are coupled to the inflaton through turns in the scalar potential or non-canonical kinetic terms. The influence of additional fields during inflation will be discussed in detail in section 1.5. Ideally, for a perfect decoupling, the rest of fields must be stabilised on *geodesic trajectories*. Specifically, if we label the fields $\Phi^a = (X, \Phi^i)$, with X being the inflaton field and Φ^i being the additional fields, they satisfy the equation of motion:

$$\ddot{\Phi}^i + \Gamma^i_{ab}\dot{\Phi}^a\dot{\Phi}^b + 3H\dot{\Phi}^i + K^{i\bar{b}}V_{\bar{b}} = 0 \ , \tag{1.4.9}$$

where $\Gamma^i_{ab} = K^{i\bar{c}}K_{ab\bar{c}}$ (see appendix A) and geodesic trajectories, or straight lines on a manifold, must satisfy:

$$\ddot{\Phi}^i + \Gamma^i_{ab}\dot{\Phi}^a\dot{\Phi}^b \propto \dot{\Phi}^i \ . \tag{1.4.10}$$

Notice that the indices a, b contain the inflaton and thus satisfying both equations above is a very non-trivial task. A possible solution [3, 82–85] is to have a *separable Kähler function* such that:

$$G(X, \bar{X}, \Phi^i, \bar{\Phi}^{\bar{i}}) = G_{\rm inf}(X, \bar{X}) + G_{\rm other}(\Phi^i, \bar{\Phi}^{\bar{i}}) \ , \tag{1.4.11}$$

which in particular implies that the metric and the Christoffel symbols are block diagonal in the inflaton-others field space. In this case, if the other fields remain on a fixed position Φ^i_0 at a critical point of the potential $V_i(X, \Phi^i_0) = 0$, they are consistently truncated and we can study their dynamics separately. The only extra requirement we need is that the critical point is actually a minimum, and not a maximum. For this one has to check that the mass matrix of the truncated sector is positive definite. This imposes constraints on the inflationary dynamics and on the parent supergravity, as we will see in detail in chapters 4 and 5.

Satisfying the critical condition $V_i(X, \Phi^i_0) = 0$ is not straightforward, as can be seen from the expression of the derivative of the scalar potential:

$$V_i = G_i V + \mathrm{e}^G \left[G^j \nabla_j G_i + G_i\right] \ . \tag{1.4.12}$$

There is a simple way to achieve $V_i(X, \Phi^i_0) = 0$, and that is by having:

$$G_i(X, \Phi^i_0) = 0 \quad \Longrightarrow \quad V_i(X, \Phi^i_0) = 0 \ . \tag{1.4.13}$$

As explained above, this implies that the fields Φ^i preserve supersymmetry, and therefore the point Φ^i_0 satisfying $G_i(X, \Phi^i_0) = 0$ is called *supersymmetric*

critical point. This configuration yields a *consistent supersymmetric truncation* of the 'non-inflating' sector [83–85]. Notice that in view of the above, only the inflaton breaks supersymmetry and therefore the inflaton is the sGoldstino [3]. The constraints on the inflationary dynamics and on the truncated sector are explored in detail in chapter 4, as well as some working examples of different inflationary scenarios that are possible in this setup.

There is yet another possible approach to achieve a decoupling of sectors during inflation. Instead of having the inflaton and the sGoldstino directions to be parallel, they can be orthogonal, as in the model with vanishing superpotential during inflation proposed in [86], where they have:

$$D_X W(X, \Phi_0^i) = 0 \quad , \quad D_i W(X, \Phi_0^i) \neq 0 \ , \tag{1.4.14}$$

where $D_a W = K_a W + W_a \neq 0$ signals supersymmetry breaking, and is equivalent to $G_a \neq 0$ for non-vanishing superpotentials. This configuration leads to $V_i(X, \Phi_0^i) = 0$ for $W(X, \Phi_0^i) = W_X(X, \Phi_0^i) = 0$, and therefore in this case the supersymmetry breaking is sourced by $W_i(X, \Phi_0^i) \neq 0$, and successful inflation with consistent decoupling can be achieved as well. We will see in chapter 5 that this situation is also constrained, since we derived the conditions of stability along the supersymmetric directions as well.

Last, let me emphasise that even when one consistently truncates the theory to the level of one dynamical complex scalar field, there are two real scalar fields and we still must be aware of the subtleties of inflation with multiple fields: turns in the trajectory, non-canonical kinetic terms, and isocurvature modes. This is precisely the subject of the next section.

1.5 Effective field theories of inflation in the presence of heavy fields

In the previous sections of this chapter we have seen how single-field slow-roll inflation models work, and how the quantum fluctuations of the inflaton field translate into the CMB temperature anisotropies. Later on, we had an overview of the motivations and difficulties to embed inflation in UV completable theories such as supergravity, where, among others, the problem of field stabilisation arises. In this section I consider the presence of multiple dynamical degrees of freedom and I analyse the conditions under which a heavy field can be consistently integrated out. Then I review the construction of effective single-field theories and how we can see the effects of the additional heavy fields from the effective single field theory point of view. Finally, we will see that even very heavy fields can leave their imprint in the correlation functions, which will be followed by chapters 2 and 3, where we make a statistical study of the significance of this kind of imprints in the CMB.

1.5.1 Inflation with multiple fields

As stressed in the previous section, in high energy theories the presence of additional fields is common. In some of the literature these fields are, explicitly or implicitly, assumed to be stabilised, and the theory is *inconsistently* truncated to a single-field description. In addition, this assumption is sometimes incorrectly justified by calculating the potential slow-roll parameters defined in (1.2.6) and (1.2.7), which ignore the presence of additional fields, because they only account for the slope and curvature of the potential in the light field direction (supposedly the inflaton). This practise results into misleading results and completely ignores the rich phenomenology conferred by the dynamics of these heavy fields.

Inflationary scenarios with multiple fields have been extensively studied, an incomplete list of works where the multiple field dynamics has been studied is [87–95] (see [96] for an excellent review). Here we will focus on the main differences with respect to the single-field case reviewed in section 1.2.

Consider a set of N real scalar fields ϕ^a, $a = 1, \ldots, N$, spanning a real manifold of dimension N with metric γ_{ab}. Similarly to the complex case seen in the previous section, the kinetic terms are given by:

$$T = \frac{1}{2}\gamma_{ab}\,\partial_\mu\phi^a\partial^\mu\phi^b \ . \tag{1.5.1}$$

The background equations of motion for the set of homogeneous scalar fields $\phi^a(t)$ in a FLRW universe are:

$$\frac{D\dot{\phi}^a}{dt} + 3H\dot{\phi}^a + \gamma^{ab}V_b = 0 \ , \tag{1.5.2}$$

where $DX^a \equiv dX^a + \Gamma^a_{bc}X^b d\phi^c$, and Γ^a_{bc} is the Levi-Civita connection associated to the metric γ_{ab}. It is useful to define a unitary vector along the trajectory:

$$T^a = \frac{\dot{\phi}^a}{\dot{\phi}} \quad , \text{ with } \quad \dot{\phi}^2 = \dot{\phi}^a\dot{\phi}_a \ . \tag{1.5.3}$$

One can also define a normal vector perpendicular to the above one in $N-1$ directions, but for the sake of simplicity we will specialise to the case of two fields. The normal vector can be defined as:

$$N^a = \epsilon^{ab}T_b \ , \tag{1.5.4}$$

where ϵ_{ab} is the Levi-Civita totally antisymmetric symbol. The normal vector N^a then satisfies[10]:

$$N_aN^b + T_aT^b = \delta^b_a \quad , \quad N^aN^b + T^aT^b = \gamma^{ab} \ . \tag{1.5.5}$$

[10]For more than two fields, we need to define the projector along the orthogonal directions to the subspace spanned by the vectors T^a and N^a, given by $P^{ab} = \gamma^{ab} - (N^aN^b + T^aT^b)$.

Then one can define the directional derivatives of the potential $V_T \equiv V_a T^a$ and $V_N \equiv V_a N^a$. If we take now the projection of the equations of motion (1.5.2) along the parallel and normal directions, we obtain, respectively:

$$\ddot{\phi} + 3H\dot{\phi} + V_T = 0 \ , \tag{1.5.6}$$

$$\frac{DT^a}{dt} = -\frac{V_N}{\dot{\phi}} N^a \ . \tag{1.5.7}$$

Notice that the first equation is analogous to that of a single-field setup, while the second signals the departure from straight trajectories, which will become relevant very soon.

Slow-roll parameters

Let us now give some definitions of slow-roll parameters in the multiple field case. The first kinematic slow-roll parameter ϵ remains the same, since it is proportional to the total kinetic energy:

$$\epsilon = -\frac{\dot{H}}{H^2} = \frac{\dot{\phi}^2}{2H^2} \ , \tag{1.5.8}$$

but the second order kinematic slow-roll parameter η_3 can be decomposed in tangential and normal components as follows:

$$\eta^a \equiv -\frac{1}{H\dot{\phi}} \frac{D\dot{\phi}^a}{dt} = \eta_{\parallel} T^a + \eta_{\perp} N^a \ , \tag{1.5.9}$$

where

$$\eta_{\parallel} = -\frac{\ddot{\phi}}{H\dot{\phi}} = 3 + \frac{V_T}{H\dot{\phi}} \quad , \quad \eta_{\perp} = \frac{V_N}{H\dot{\phi}} = \frac{\dot{\theta}}{H} \ . \tag{1.5.10}$$

Note that the parallel component coincides with the single-field definition η_3 in (1.2.4). Let me stress that $\eta_{\perp} \neq 0$ signals a turn in the inflationary trajectory, with $\dot{\theta}$ being the turn rate, and that it does not necessarily have to be small, so in that sense $\eta_{\perp}$ is not a slow-roll parameter but a slow-turn parameter.

As for the potential slow-roll parameter ϵ_V, the definition for the multiple field case has to incorporate the slope of the potential in all the field directions, since the inflaton will always roll in the steepest direction, and therefore it reads:

$$\epsilon_V = \frac{1}{2V^2} \gamma^{ab} V_a V_b = \frac{1}{2} \left(\frac{V_T}{V} \right)^2 \left[1 + \left(\frac{V_N}{V_T} \right)^2 \right] \ , \tag{1.5.11}$$

which can be rewritten using the definitions in (1.5.10) as follows:

$$\epsilon_V = \frac{\epsilon}{(3-\epsilon)^2} \left[(3 - \eta_{\parallel})^2 + \eta_{\perp}^2 \right] \ . \tag{1.5.12}$$

Notice that for straight trajectories, $\eta_\perp = 0$, and the expression above reduces to the single-field parameter, as it should. Once we have these quantities at hand, let us turn to the phenomenological aspects.

Adiabatic and isocurvature (or entropy) perturbations

In this subsection our purpose is to explain that in the presence of multiple fields, isocurvature (or entropy) perturbations are not necessarily suppressed, and they might spoil the conservation of the adiabatic curvature perturbation on large scales, as opposed to the single field case. In the following I will review the main qualitative results of the analysis in [88].

For the purpose of this section, we will consider a set of scalar fields ϕ^a with canonical kinetic terms, i.e. the metric of the field manifold is the identity. I will denote field indices with the first letters of the alphabet $(a, b, \dots)$ and coordinate indices with the middle letters $(i, j, \dots)$. When considering linear perturbation of scalar fields, one must also consider metric perturbations, which can be parameterised as follows:

$$ds^2 = -(1+2A)\,dt^2 + 2a\partial_i B\,dx^i dt + a^2\left[(1-2\psi)\delta_{ij} + 2\partial_i\partial_j E\right]\,dx^i dx^j \ , \quad (1.5.13)$$

where the partial derivatives ∂_i denote derivatives with respect to the coordinates. Considering perturbations of the scalar fields of the form $\phi^a \to \phi^a(t) + \delta\phi^a(\mathbf{x}, t)$, the equations of motion in Fourier space read:

$$\begin{aligned}\delta\ddot{\phi}^a + 3H\delta\dot{\phi}^a + \frac{k^2}{a^2}\delta\phi^a + \delta^{ab}V_{bc}\delta\phi^c = -2A\delta^{ab}V_b \\ +\dot{\phi}^a\left[\dot{A} + 3\dot{\psi} + \frac{k^2}{a^2}\left(a^2\dot{E} - aB\right)\right] \ ,\end{aligned} \quad (1.5.14)$$

where the subindices denote derivatives with respect to the fields, and the background fields $\phi^a(t)$ satisfy the equations of motion (1.5.2) with a trivial field metric. Let us now define the comoving curvature perturbation (in the longitudinal gauge):

$$\mathcal{R} = \psi - \frac{H}{\dot{H}}\left(\dot{\psi} + HA\right) \ , \quad (1.5.15)$$

which is related to the curvature perturbation on uniform density hypersurfaces ζ as follows:

$$-\zeta = \mathcal{R} + \frac{2\rho}{3(p+\rho)}\left(\frac{k}{aH}\right)^2\psi \quad \xrightarrow{k\ll aH} \quad \mathcal{R} \ . \quad (1.5.16)$$

We will soon see that both $\mathcal{R}$ and ζ remain constant at large (superhorizon) scales for purely adiabatic perturbations. Since in this thesis we will focus on effectively single field inflation, and we will be mostly interested on the behaviour of correlation functions on superhorizon scales, I will often abuse the language

and refer to both of them as adiabatic curvature perturbation.

One can also define the (gauge-independent) total entropy perturbation by splitting the pressure perturbation in adiabatic and entropic parts:

$$\delta p = \frac{\dot{p}}{\dot{\rho}}\delta\rho + \frac{\dot{p}}{H}\mathcal{S} \quad , \quad \text{with} \quad \mathcal{S} = H\left(\frac{\delta p}{\dot{p}} - \frac{\delta\rho}{\dot{\rho}}\right) . \tag{1.5.17}$$

It can be shown [97] that on large scales, due to local energy conservation, the variation in the adiabatic curvature perturbation is

$$\dot{\mathcal{R}} = -3H\frac{\dot{p}}{\dot{\rho}}\mathcal{S} , \tag{1.5.18}$$

and therefore when the pressure perturbation is adiabatic ($\mathcal{S} = 0$), $\mathcal{R}$ is conserved on superhorizon scales. Let us evaluate the entropy perturbation for the cases of single-field and two-field inflation.

For **single-field**, since the scalar field φ is determined up to two integration constants, they describe adiabatic and entropic perturbations. It can be seen that in the longitudinal gauge the entropy perturbation can be written as:

$$\mathcal{S} = -\frac{V_\varphi}{6\pi G\dot{\varphi}^2\left(3H\dot{\varphi} + 2V_\varphi\right)}\left(\frac{k^2}{a^2}\psi\right) \quad \Longrightarrow \quad \dot{\mathcal{R}} = \frac{H}{\dot{H}}\frac{k^2}{a^2}\psi \quad \xrightarrow{k\ll aH} \quad 0 , \tag{1.5.19}$$

and therefore the curvature perturbation is conserved on large scales.

For **two-field** inflation, as explained above, one can choose a basis in field space such that one of the directions is parallel to the trajectory (adiabatic field) and the other direction perpendicular (entropy field). In order to facilitate the connection with [88], I will keep their notation unchanged, except for the quantities introduced in this text previously. The adiabatic and entropy fields can be defined as:

$$\dot{\phi} = T^a\dot{\phi}_a \quad , \quad \delta s = N^a\delta\phi_a , \tag{1.5.20}$$

where ϕ_a is the vector of two fields, and the tangential and normal unitary vectors (T^a, N^a) were defined in (1.5.3) and below. The entropy perturbation is then given by:

$$\mathcal{S} = -\frac{V_T}{6\pi G\dot{\phi}^2\left(3H\dot{\phi} + 2V_T\right)}\left(\frac{k^2}{a^2}\psi\right) - \frac{2V_N}{3\dot{\phi}^2}\delta s , \tag{1.5.21}$$

where an additional contribution coming from the entropy field proportional to the turn rate[11] $\dot{\theta} = V_N/\dot{\phi}$ appears at all scales. Due to this, the change in the

[11] Note the slight change of notation with respect to [88], where the turn rate is defined as $\dot{\theta} = -V_N/\dot{\phi}$.

adiabatic curvature perturbation receives an extra contribution of the form:

$$\dot{\mathcal{R}} = \frac{H}{\dot{H}}\frac{k^2}{a^2}\psi - \frac{2H}{\dot{\phi}}\dot{\theta}\delta s \ . \tag{1.5.22}$$

Here we clearly see how the presence of an additional field might produce superhorizon evolution of the adiabatic curvature perturbation, which is in disagreement with experiments. Despite of this, a large effective mass for the entropy field will suppress the entropy perturbation at superhorizon scales.

At the level of the equations of motion, both modes decouple for $\dot{\theta} = 0$, as one would expect. In fact, on large scales the entropy perturbation satisfies a homogeneous second order equation, however the adiabatic perturbation suffers from metric back-reaction and a source term coming from the entropy perturbation. This can be seen in the power spectrum, since the entropy perturbation enhances the adiabatic spectrum, but not vice versa.

To summarise, we have seen that when multiple fields participate on inflation, the only way to suppress isocurvature or entropy perturbations is to have straight trajectories and a heavy mass in the perpendicular direction, such that the entropy fluctuations do not survive at late times, unless there is a particular mechanism that avoids the generation of isocurvature perturbations. Note that non-canonical kinetic terms may cause the same turning effects on trajectories that would otherwise look straight. In the next subsection we will see some of these aspects in more detail, but formulated slightly different, in such a way that it permits us to establish direct connection with the effective field theory of inflation [98]. From now on we will focus on inflationary models that can be described by a single field after integrating out the heavy degrees of freedom. We will discuss the conditions under which this integration is valid and the fingerprints of the heavy physics on the low-energy effective theory.

1.5.2 Effective single-field inflation and the speed of sound

We will now focus on inflation with a light field and a heavy field and review the construction of an effective field theory for the light field. There has been extensive work in the last decade in this respect, for instance see [98–110] for work related to effective single-field theories and the integration of heavy fields.

Let us consider a set of N real scalar fields ϕ^a spanning a manifold with metric γ_{ab}. The kinetic energy of the fields is given by (1.5.1) and their equations of motion by (1.5.2). We parameterise the perturbations around the background solution $\phi_0^a(t)$ as indicated in figure 1.9: the field $\pi(t, \mathbf{x})$ represents displacements along the background trajectory, while $\mathcal{F}(t, \mathbf{x})$ parameterises deviations off the background trajectory along the perpendicular direction N^a at the time

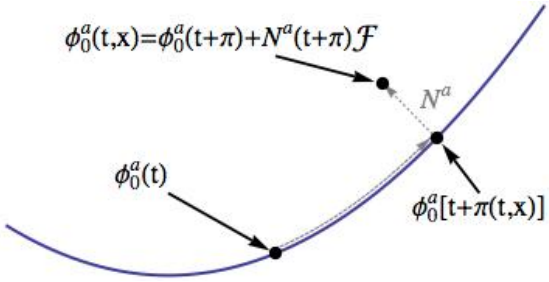

Figure 1.9 *– Parameterisation of perturbations along the background trajectory, using the displacement along the trajectory, π, and the unitary vector orthogonal to the background trajectory, N^a. The displacement in the orthogonal direction is proportional to the heavy mode $\mathcal{F}$. Figure adapted from [107].*

$t + \pi$. Intuitively, one would think that π is related to the adiabatic curvature perturbation $\mathcal{R}$ and $\mathcal{F}$ to the entropy perturbation $\mathcal{S}$, and indeed this is the case, because $\mathcal{R} = -\pi H$ [39] and $\mathcal{F} = \mathcal{S}\dot{\phi}_0/H$ (see, for instance [106]). We will work in terms of $\mathcal{R}$ and $\mathcal{F}$ to respect the notation of [106, 107].

In terms of $\mathcal{R}$ and $\mathcal{F}$, the quadratic action reads:

$$S_2 = \int d^4x \left[\frac{\dot{\phi}_0^2}{H^2}\dot{\mathcal{R}}^2 - \frac{\dot{\phi}_0^2}{H^2}\frac{1}{a^2}(\nabla\mathcal{R})^2 + \dot{\mathcal{F}}^2 - \frac{1}{a^2}(\nabla\mathcal{F})^2 + 4\dot{\phi}_0^2\eta_\perp\dot{\mathcal{R}}\mathcal{F} - M_{\rm eff}^2\mathcal{F}^2 \right] , \tag{1.5.23}$$

where $M_{\rm eff}^2 = V_{NN} + H^2\epsilon\mathbb{R} - \dot{\theta}^2 = m^2 - \dot{\theta}^2$ is interpreted as the mass of the heavy field $\mathcal{F}$, and $\mathbb{R}$ is the Ricci scalar of the field manifold. The equations of motion derived from the action above are:

$$\begin{aligned} \ddot{\mathcal{R}} + \left(3 + 2\epsilon - 2\eta_\parallel\right) H\dot{\mathcal{R}} - \frac{1}{a^2}\nabla^2\mathcal{R} &= -\frac{2H^2}{\dot{\phi}_0}\eta_\perp\left[\dot{\mathcal{F}} + \left(3 - \eta_\parallel - \xi_\perp\right) H\mathcal{F}\right] , \\ \ddot{\mathcal{F}} + 3H\dot{\mathcal{F}} - \frac{1}{a^2}\nabla^2\mathcal{F} + M_{\rm eff}^2\mathcal{F} &= 2\dot{\phi}_0\eta_\perp\dot{\mathcal{R}} , \end{aligned} \tag{1.5.24}$$

where $\xi_\perp = -\dot{\eta}_\perp/\eta_\perp H = -\ddot{\theta}/\dot{\theta}H - \epsilon$ is related to the turn acceleration. We can now clearly see that the equations of motion are coupled whenever $\eta_\perp \neq 0$, or in other words, when the inflationary trajectory traverses a turn.

Decoupling

The equations of motion (1.5.24) can be interpreted as two coupled harmonic oscillators with a derivative coupling, for which one can propose the ansatz:

$$\mathcal{F}(\mathbf{k}, t) = f(\mathbf{k})\mathrm{e}^{i\omega t} \quad , \quad \mathcal{R}(\mathbf{k}, t) = r(\mathbf{k})\mathrm{e}^{i\omega t} . \tag{1.5.25}$$

Let us take the slow-roll ($\epsilon, \eta_{\parallel} \ll 1$) and soft-turn ($\xi_{\perp} \ll 1$) limit, and disregard Hubble friction terms. Under those assumptions, the equations of motion in Fourier space can be approximated by:

$$\ddot{\mathcal{R}} + \frac{k^2}{a^2}\mathcal{R} = -\frac{2H}{\dot{\phi}_0}\dot{\theta}\dot{\mathcal{F}} \ ,$$

$$\ddot{\mathcal{F}} + \frac{k^2}{a^2}\mathcal{F} + M_{\rm eff}^2\mathcal{F} = 2\dot{\phi}_0\frac{\dot{\theta}}{H}\dot{\mathcal{R}} \ . \tag{1.5.26}$$

Plugging the ansatz (1.5.25) into the simplified equations of motion (1.5.26) we obtain the following equation for the frequencies:

$$\omega^4 - \omega^2\left(4\dot{\theta}^2 + \frac{2k^2}{a^2} + M_{\rm eff}^2\right) + \frac{k^2}{a^2}\left(\frac{k^2}{a^2} + M_{\rm eff}^2\right) = 0 \ , \tag{1.5.27}$$

whose solution is given by:

$$\omega_{\pm}^2 = \frac{1}{2}\left[\left(4\dot{\theta}^2 + \frac{2k^2}{a^2} + M_{\rm eff}^2\right) \pm \sqrt{\left(4\dot{\theta}^2 + M_{\rm eff}^2\right)^2 + 16\dot{\theta}^2\frac{k^2}{a^2}}\ \right] \ , \tag{1.5.28}$$

which is the result displayed in [102, 109]. Hence, the solutions for the curvature and isocurvature modes in (1.5.25) will be a linear combination of heavy modes of frequency ω_+ and light modes of frequency ω_-:

$$\mathcal{F}(\mathbf{k}, t) = f_+(\mathbf{k})\mathrm{e}^{i\omega_+ t} + f_-(\mathbf{k})\mathrm{e}^{i\omega_- t} \ ,$$

$$\mathcal{R}(\mathbf{k}, t) = r_+(\mathbf{k})\mathrm{e}^{i\omega_+ t} + r_-(\mathbf{k})\mathrm{e}^{i\omega_- t} \ , \tag{1.5.29}$$

where the relation between the amplitude of different modes can be found by substituting our ansatz in the equations of motion, and is given by:

$$\frac{r_{\pm}}{f_{\pm}} \simeq \frac{2iH\dot{\theta}\omega_{\pm}}{\dot{\phi}_0\left(\omega_{\pm}^2 - \frac{k^2}{a^2}\right)} \ , \tag{1.5.30}$$

or equivalently:

$$\frac{f_{\pm}}{r_{\pm}} \simeq -\frac{2i\dot{\phi}_0\dot{\theta}\omega_{\pm}}{H\left(\omega_{\pm}^2 - \frac{k^2}{a^2} - M_{\rm eff}^2\right)} \ . \tag{1.5.31}$$

At this point one can study all the different hierarchies between the parameters k/a, $M_{\rm eff}$ and $\dot{\theta}$, which will tell us in what limit the modes are decoupled, that is, when $f_+ \gg r_+$ and $f_- \ll r_-$ the mode $\mathcal{F}$ is mostly heavy with frequency $\omega_+ \gg \omega_-$, and the mode $\mathcal{R}$ is mostly light with frequency $\omega_- \ll \omega_+$. This happens in particular for $M_{\rm eff} \gg k/a, \dot{\theta}$, and surprisingly for $\dot{\theta} \gg H, k/a$.

As emphasised in [109], one would expect that for a large turn rate, the effective mass of the heavy field decreases and therefore the modes would not decouple. However, one observes that a large turn rate helps in mode decoupling, i.e. the gap between the frequencies $\omega_{\pm}$ increases. In the following I will describe the conditions under which the heavy field can be integrated out, so that one can write down an effective single field theory for the adiabatic curvature perturbation under the effects of the heavy mode.

Integrating out $\mathcal{F}$ and the sound speed

We focus now on the equation of motion for the heavy mode in (1.5.24). We will stick to the regime in which $M_{\rm eff} \gg H$ so that we can disregard isocurvature fluctuations, and also neglect the friction term in the equation of motion (1.5.24). Then, in the regime where $|\ddot{\mathcal{F}}| \ll M_{\rm eff}^2 |\mathcal{F}|$, in which the kinetic terms of $\mathcal{F}$ can be neglected, we can express the entropy (heavy) field in terms of the adiabatic (light) field as follows:

$$\mathcal{F}_{\mathcal{R}} = \frac{2\dot{\phi}_0 \eta_{\perp}}{k^2/a^2 + M_{\rm eff}^2} \dot{\mathcal{R}} \ . \tag{1.5.32}$$

Plugging this solution into the quadratic action (1.5.23) we find the following effective action for the adiabatic mode (see [107] for a elaborated treatment):

$$S_{\rm eff,2} = \int d^4x \, a^3 \epsilon \left[\frac{\dot{\mathcal{R}}^2}{c_s^2} - \frac{(\nabla \mathcal{R})^2}{a^2} \right] \ , \tag{1.5.33}$$

where we have defined the *speed of sound* of the adiabatic mode:

$$c_s^{-2} = 1 + \frac{4\dot{\theta}^2}{k^2/a^2 + M_{\rm eff}^2} \ . \tag{1.5.34}$$

Some important points are to be made here:

- Whenever the inflationary trajectory traverses a turn, from the effective field theory point of view it appears as a reduction in the speed of sound of the adiabatic mode. Isolated turns translate into transient reductions of the speed of sound.
- Reductions in the speed of sound are completely consistent with a slow-roll regime.
- Transient reductions in the speed of sound result into localised features in the power spectrum, which is evident from the presence of c_s^{-2} in the quadratic action. This happens as well for higher order correlation functions. In fact, in chapters 2 and 3 we will also show the effective cubic action and calculate the features both in the power spectrum and bispectrum. These can be calculated using the in-in formalism and considering the contribution

of the reduced speed of sound as a perturbation, as we will see in detail in chapter 3.

- Given that the speed of sound appears at all orders in the effective action, the features in the correlation functions are correlated [111, 112].

- The validity of the effective field theory is subject to the adiabatic condition $|\ddot{\mathcal{F}}| \ll M_{\rm eff}^2 |\mathcal{F}|$, which in terms of background quantities can be written as [106]:

$$\left| \frac{d}{dt} \ln(1 - c_s^{-2}) \right| \ll M_{\rm eff} \ , \tag{1.5.35}$$

  which essentially implies that turns cannot be too sudden (large angular acceleration), but they can still be strong (large angular turn rate).

To summarise the material presented in this section, we have seen that the presence of multiple fields during inflation produces a rich phenomenology. While the production of entropy fluctuations is dangerous, it is nevertheless possible to suppress them if the entropy field is sufficiently heavy. In that case, one can construct an effective single field theory for the adiabatic curvature perturbation, where the effect of the heavy physics is parameterised in terms of a reduced speed of sound for the adiabatic mode. The single-field description is valid as long as turns along the inflationary trajectory are not too sudden, and transient reductions of the speed of sound reveal themselves through localised features in the correlation functions. This has important consequences, since it opens a window to detect the presence of heavy fields during inflation. In fact, in chapter 2 I present the work in which we performed a search for this kind of features in the Planck CMB data, and in chapter 3 I present an elaborated treatment of the calculation of these features using different methods, and the consistency of the effective field theory.